ELSEVIER

Spectrochimica Acta Part B 52 (1997) 1663–1686

SPECTROCHIMICA ACTA PART B

An investigation of the 2f—wavelength modulation technique for detection of atoms under optically thin as well as thick conditions

Dorys Rojas[1], Per Ljung, Ove Axner*

Department of Experimental Physics, Umeå University, S-901 87 Umeå, Sweden

Received 15 November 1996; accepted 8 April 1997

Abstract

An investigation of the *2f*-wavelength modulation (WM) technique for detection of atoms under optically thin as well as thick conditions is presented. A program that simulates the entire process of laser light modulation, atomic absorption and signal demodulation has been constructed. The dependence of the *2f*-WM signal upon frequency amplitude modulation and detuning for a variety of atomic masses (i.e. optical densities) is investigated in detail. It is shown, among other things, that the *2f*-WM ($\bar{S}_{2f-r}$) signal strength is either a dual- or a quadrupled-valued function of optical density. Despite this, it shown that the *2f*-WM technique can be used, by suitable choices of the frequency amplitude modulation and detuning, for detection of atoms also under optically thick conditions. © 1997 Elsevier Science B.V.

Keywords: Wavelength modulation; *2f*-WM; Voigt; Optically thick conditions; Element detection; Rubidium; Diode lasers

1. Introduction

It is well-known that the detection ability of trace species in gas phase by laser-based spectroscopic techniques often can be significantly improved by the use of various modulation techniques [1,2]. The general approach comprises of modulating the frequency (or the wavelength) of the laser light prior to interaction with the species to be detected. The experimental signal (e.g. in the case of absorption: the current from a photodiode) is then extracted from the modulated signal by a suitable homodyne technique (most often processed by a lock-in amplifier). This process significantly reduces noise and drifts (e.g. from the laser or the atomizer, changes of index of refraction from the surrounding atmosphere, etc) by shifting the detection to higher frequencies were drifts are less significant. It also removes baseline off-sets, slopes or even some curvature of the background (depending on the mode of operation, see further discussion below).

Wavelength Modulation (WM) spectroscopy is the most commonly used technique for improving trace species detection in absorption mode [1]. There are several different means of utilizing WM-techniques. The most commonly is to use *2f*-detection (i.e. to modulate the wavelength of the laser source at one frequency, f_m, and then detect the absorption by the use of a lock-in amplifier whose reference signal has a frequency of twice this frequency, $2f_m$, see further

* Corresponding author. Fax: +46 90 16 66 73; internet: http://www.phys.umu.se/laser.

[1] On temporary leave from: Department of Chemistry, Faculty of Science, University of the Andes, Merida, Venezuela (FAX: + 58 74 401286).

PII S0584-8547(97)00056-6

discussion below) [3]. Sensitivities around 10^{-4}–10^{-5} (fractional absorbances) have repeatedly been observed [2,4–9]. Even lower sensitivities have been obtained from WM-techniques in combination with extensions of this technique (e.g. modulation of also the atomizer) [10].

It has been tacitly assumed that the *2f*-output signal from the lock-in amplifier is directly proportional to the number of traces species in the interaction region. This is, however, only valid for optically thin media. It is important to detect atoms not only under optically thin conditions.

It is not a problem, in general, to detect traces under (or close to) optically thick conditions in flames of furnaces. The two most commonly used means to handle samples with higher concentrations are either to dilute the sample or to use alternative transitions (with a lower sensitivity). Sample dilution can, however, involve quite an elaborate procedure if a set of samples with unknown and largely varying concentrations of traces is to be analyzed. In addition, all sample pretreatment procedures infer an increased risk for contamination. It is, therefore, a strive in the development of analytical instrumentation to reduce sample pretreatment procedures as much as possible. Moreover, the use of less sensitive transitions for detection of elements is not trivial for diode-laser based techniques since it requires access to a large variety of diode lasers (since less sensitive transitions only occasionally can be found within the working range of diode laser used for detection on a strong transition).

We have therefore, in this paper, studied the applicability of the *2f* WM-technique to more general conditions (i.e. both optically thin and thick conditions). This has been done by a numerical simulation of the entire modulation-interaction-and-detection process. Hence, this paper is concerned with an investigation of the possibilities to use the *2f* WM-technique for detection of atoms under both optically thin and thick (steady-state) conditions. This paper is the first in a series that investigate the properties of the *2f* WM-technique for detection of atoms under such conditions.

A second paper in this series is concerned with an investigation of the influence of hyperfine as well as isotope structure of the atoms (exemplified with Rb) on the *2f* WM-technique [11].

The third paper is concerned with extension of the dynamic range of the *2f* WM-technique (the WM-LDAS-GF technique) to detection of atoms under optically thick non-steady state conditions (e.g. in graphite furnaces in which there is not even a constant temperature by necessity) [12]. In addition, the fact that the *2f* WM-technique detects the 'curvature' of the absorption profile (rather then the absorption profile itself) makes it potentially vulnerably to changes in the temperature (since the combined Voigt profile consists of a Gaussian and a Lorentzian function whose temperature dependencies are inverse to each other). The temperature dependence of the *2f*-WM technique is therefore also investigated in the accompanying paper [12].

The present paper is structured as follows. First, a general but quite thorough description of the wavelength modulation technique is given (in which the *2f* WM-technique is scrutinized in more detail). This is followed by simulations of *2f*-detection of atoms under optically thin as well as thick conditions for a variety of conditions. It is shown that the technique is capable of detecting species under both optically thin and thick conditions. This property thus vouches for an eminently large dynamic range of the *2f* WM-technique [12].

2. General description of wavelength modulation techniques

2.1. General principles and procedures of wavelength modulation techniques

2.1.1. Wavelength modulation

Wavelength modulation techniques is build upon a modulation of the laser light wavelength, λ, by a sinusoidal modulation frequency, f_m

$$\lambda(t) = \lambda_c + \lambda_{\mathrm{mod}} \sin(2\pi f_m t) \tag{1}$$

where λ_c is the center wavelength and λ_{mod} is the wavelength modulation amplitude. For diode laser spectroscopy, which is the most commonly used area for the WM spectrometric techniques, this implies a corresponding sinusoidal modulation of the injection current.

Since it is more customary to work with broadening and distribution functions in frequency space than in

wavelength space, the modulation can more conveniently be written in terms of frequency (i.e. in units of Hz):

$$\nu(t) = \nu_c + \nu_{\mathrm{mod}} \sin(2\pi f_m t) \tag{2}$$

where ν_c is the center frequency and ν_{mod} is the frequency modulation amplitude.

We have here adopted the convention that the modulation frequency (which is of electrical origin) is written with Arabic, italic font, i.e. f, while light frequencies appear in Greek, italic font, i.e. ν.

2.1.2. Time-dependent absorption signals

For absorption techniques, it is also well-known that the absorption of narrowbanded light (e.g. from a hollow cathode lamp or a diode laser), A, defined as the relative decrease of the intensity of the diode laser light of the absorption profile, can be written as

$$A = \frac{I_0 - I}{I_0} = 1 - e^{-\rho L \sigma} \tag{3}$$

where I_0 and I are the laser light intensities prior to and after the interaction region, respectively, ρ is the density of species to be detected, L the interaction length, and σ the absorption cross-section (normally at the peak of the absorption profile).

When wavelength modulated techniques are employed, or when the absorption profile is measured by diode laser spectroscopy, also the *shape* of the line profile is of importance for evaluation of atomic densities from the signal. This can most conveniently be accounted for by assigning a profile shape to the absorption cross-section, e.g. as follows:

$$\sigma(\nu) = \sigma_0 \frac{\chi(\nu)}{\chi_0} \tag{4}$$

where σ_0 represents the absorption cross-section at the peak of the profile, i.e. $\sigma(\nu_0)$, $\chi(\nu)$ the line-shape function for the species to be detected and χ_0 the (peak) value of the line-shape function, i.e. $\chi(\nu_0)$. It is well-known that the line-shape function, $\chi(\nu)$, in general, constitutes of a Voigt profile, below referred specifically to as $V(\nu)$ [which in turn originates from a combination of a homogeneous broadening of Lorentzian type, $L(\nu)$, and an inhomogeneous broadening of Gaussian type, $G(\nu)$]. Thus, we have in this presentation chosen to explicitly show that the absorption cross-section has a frequency dependence.

In addition, since the shapes of the line profile are of importance for evaluation of atomic densities from the *2f*-WM signals, it is also plausible that the technique also has a certain temperature dependence (since the Lorentz and a Gaussian profiles have weak but different temperature dependencies, with widths roughly scaling as T^n and T^{-n}, respectively, with n most often in the interval [0, 0.5]). This concept can therefore be of importance when atoms are to be detected under non-steady state temperature conditions, e.g. in the leading part of the atomization curve in a graphite furnace. This concept is, however, investigated in more detail in a separate paper [12]. We have therefore in this paper restricted the analysis to temperature steady-state conditions.

The *instantaneous absorption* (when the incident light is modulated around a center frequency ν_c, according to Eq. (2)) from a distribution of atoms (an atomic density of ρ distributed over an interaction length of L) is then given by

$$A(t) = 1 - \exp\left[-\rho L \sigma_0 \frac{\chi(\nu_c + \nu_{\mathrm{mod}} \sin(2\pi f_m t))}{\chi_0}\right] \tag{5}$$

where the appropriate line-shape function is to be inserted into the expressions above for $\chi(\nu)$. As an example, for the case of a pure Lorentzian broadening,

$$L(\nu) = \frac{1}{2\pi\Delta\nu_L} \frac{(\Delta\nu_L)^2}{(\nu_0 - \nu)^2 + (\Delta\nu_L)^2} \tag{6}$$

the time dependent line-shape function looks like

$$\chi(\nu(t)) = L(\nu_c + \nu_{\mathrm{mod}} \sin(2\pi f_m t)) = \frac{1}{2\pi\Delta\nu_L} \frac{(\Delta\nu_L)^2}{(\nu_0 - \nu_c - \nu_{\mathrm{mod}} \sin(2\pi f_m t))^2 + (\Delta\nu_L)^2} \tag{7}$$

(where $\Delta\nu_L$ is the Half-Width-Half-Maximum of the Lorentzian profile for the pertinent experimental conditions and ν_0 the atomic transition frequency), with similar expressions for the pure Gaussian or the combined Voigt profile.

This implies that the *instantaneous detector signal*, $S_{d.s.}$ (ν_c,t), can be written

$$S_{d.s.}(\nu_c, t) = \kappa[1 - A(t)]I_0 = \kappa I_0 \exp\left[-\rho L \sigma_0 \frac{\chi(\nu_c + \nu_{\mathrm{mod}} \sin(2\pi f_m t))}{\chi_0}\right] \tag{8}$$

where κ is an instrumentation constant (including a photodiode response and an amplification function) that relates the measured signal (in Volt) to the light intensity impinging upon the photodiode (W).

2.1.3. Harmonic processing

Finally, by multiplying the modulated detector signal with another sinusoidal function, $S_{ref}(t)$, (often referred to as a reference signal or a read-out signal) whose frequency is an integer multiple, n, of the modulation signal, i.e.

$$S_{ref}(t) = \sin(2\pi\, nf_m t) \tag{9}$$

and taking the average over a suitable number of periods (which very conveniently can be done by a lock-in amplifier), here represented by an integration over a suitable amount of time, τ, the final nf-WM signal, $\bar{S}_{nf}$, results:

$$\bar{S}_{nf}(\nu c) = \frac{1}{\tau}\int_0^{\tau} S_{ref}(t)\cdot S_{d.s.}(\nu_c, t)dt. \tag{10}$$

One has the choice of selecting any (suitable) phase relation between the modulated detector signal and the reference signal. It is often convenient to chose this phase factor equal to an integer multiple of $\pi/2$ (i.e. 0, $\pi/2$, π, etc.). The terms 'in-phase' and 'out-of-phase' signals, or x- and y-components, are often used for the cases when the phase angles are chosen as 0 and $\pi/2$, respectively:

$$\bar{S}_{nf-x}(\nu_c) = \frac{1}{\tau}\int_0^{\tau} \sin(2\pi n f_m t) \times S_{d.s.}(\nu_c + \nu_{\mathrm{mod}} \sin(2\pi f_m t))dt \tag{11}$$

$$\bar{S}_{nf-y}(\nu_c) = \frac{1}{\tau}\int_0^{\tau} \sin(2\pi n f_m t + \pi/2) \times S_{d.s.}(\nu_c + \nu_{\mathrm{mod}} \sin(2\pi f_m t))dt \tag{12}$$

It is also possible to express the resulting signal in complex form, i.e. with an amplitude and a phase-angle. The amplitude, which normally is termed the 'r-component', can thus be created simply as the square root of the sum of the squares of the 'x-' and 'y-components,' i.e.

$$\bar{S}_{nf-r}(\nu_c) = \sqrt{(\bar{S}_{nf-x}(\nu_c))^2 + (\bar{S}_{nf-y}(\nu_c))^2} \tag{13}$$

Arndt [13] has shown that the signal strength of the nth harmonic can be expressed in terms of an integral as

$$\bar{S}_{nf}(\nu_c) = \frac{(-1)^n(2-\delta_{n0})}{\pi} \times \int_{-\nu_{\mathrm{mod}}}^{\nu_{\mathrm{mod}}} S(\nu_c - \nu')\, \frac{T_n(\nu'/\nu_{\mathrm{mod}})}{\sqrt{(\nu_{\mathrm{mod}})^2 - (\nu')^2}} d\nu' \tag{14}$$

where δ_{n0} is the Kronecker delta (i.e. $\delta_{n0} = 1$ if $n = 0$, $\delta_{n0} = 0$ otherwise) and T_n is the Chebyshev polynomial of degree n.

2.1.4. Scanning procedure

In order to scan across a peak (so as to study the shape of the profile), the laser output frequency needs to be modulated not only by the sinusoidal wavelength modulation function (which normally is in the kHz range), but also by a linear ramp (considerably slower, often in the Hz range). One can see this as if the center frequency, around which the rapid sinusoidal wavelength modulation takes place, is slowly shifted, e.g.

$$\nu_c(t) = \nu_{start} + (\nu_{end} - \nu_{start})\frac{t}{\tau_{ramp}} \quad for\ 0 \le t < \tau_{ramp} \tag{15}$$

where τ_{ramp} represents the period of the ramp (i.e. the inverse of the ramp frequency), $(\nu_{end} - \nu_{start})$ the ramp length (in units of GHz) and where $(\nu_{end} - \nu_{start})/\tau_{ramp}$ represents the ramp rate (GHz/s).

It this customary to choose this ramping period sufficiently long with respect to the smoothing period, τ (since otherwise a significant part of the structural information, i.e. the line profile, will be smoothened out).

In the limit of small frequency modulation amplitudes (i.e. small ν_{mod}), the line shape of the *nth* harmonic is proportional to the *nth* derivative of the line shape (hence the use of the term 'second order derivative spectroscopy' of the technique when the *2f* harmonic is being processed).

2.2. Second harmonic modulation

It is possible to perform wavelength modulation by measuring, in principle, any harmonic of the modulated signal. For example, Arndt calculated line

shapes (analytically) for the 1st and 2nd harmonic (i.e. $n = 1$ and 2) for a pure Lorentzian profile [13], Cassidy and Reid calculated relative peak heights for the 2nd, 4th, 6th, and 8th harmonic of a pure Lorentzian profile [4], Wilson used numerical integration to obtain the three first harmonics of both Gaussian and Lorentzian profiles [14], while Silver determined the optimum values of the modulation index (m) for both Gaussian and Lorentzian profiles for the 1st, 2nd, 4th, and 6th harmonic [1], where the modulation index, m, is defined as the ratio of the amplitude of the modulation amplitude, ν_{mod}, to the Half-Width-Half-Maximum (HWHM) of the unmodulated line profile function, in our case $\Delta\nu_{S_{dc}(\nu mod=0)}$. Silver found that the optimum modulation index was 1.6 and 2.0 for first harmonic detection of pure Gaussian and Lorentzian profiles, respectively. The corresponding modulation indices for second, forth and sixth harmonic detection were (2.1 and 2.2), (3.6 and 3.9), and (5.2 and 7.4) (for pure Gaussian and Lorentzian profiles, respectively).

It has been quite commonplace, however, to detect the second harmonic output (the *2f*-signal). One reason for this is that the *2f*-output eliminates (or reduces significantly) both constant or linearly sloping baselines (since the signal strength is more or less proportional to the second derivative of the profile). Another is that the signal (under optically thin conditions) peaks at the absorption line center for pure Lorentzian, Gaussian, and Voigt profiles.

2f-detection has been scrutinized in more detail by Arndt [13] as well as Reid and Labrie [3]. Their calculations of the line shapes for the second harmonic output for a pure Lorentzian absorption profile under low optical density conditions (i.e. when $\rho L\sigma < 1$) revealed that the second harmonic signal strength ($\bar{S}_{nf-y}(\nu_c)$) can be written

$$\bar{S}_{nf-y}(\nu_c) = \kappa I_0[1 - H_2^L(x,m)] \tag{16}$$

where

$$H_2^L(x,m) = \frac{4}{m^2}\left[1 - \frac{(M+1-x^2)\sqrt{\sqrt{M^2+4x^2}+M} + 4x\sqrt{\sqrt{M^2+4x^2}-M}}{2\sqrt{2}\sqrt{M^2+4x^2}}\right] \tag{17}$$

where

$$M = 1 - x^2 + m^2 \tag{18}$$

and x is the half-width-normalized-detuning

$$x = \frac{\nu_c - \nu_0}{\Delta\nu_L} \tag{19}$$

In the limit of small modulation index (i.e. small m), the expression above reduces to

$$H_2^L(x, m \to 0) = \frac{m^2}{4}\cdot\frac{6x^2-2}{(1+x^2)^3} + O(m^4) \tag{20}$$

which clearly is proportional to the second order derivative of the Lorentz function (Eq. (6)), which reads

$$\frac{\partial^2 L(\nu)}{\partial\nu^2} = \frac{1}{2\pi\Delta\nu_L}\frac{6x^2-2}{(1+x^2)^3} \tag{21}$$

The second harmonic signal strength for pure Gaussian and Voigt profiles (given in terms of an integral) have been calculated by Reid and Labrie [3]. The same authors also calculated peak heights as functions of the modulation index m for pure Lorentzian, Gaussian as well as Voigt profiles for *2f*-detection.

In order to be able to predict the *2f*-signal response (the shape as well as the signal strengths of the *2f*-profiles) not only for optically thin conditions (which seems not to have been done before), so as to assess the full applicability of the technique for detection of atomic species in both low and high optical densities, the signal generation and detection system has been simulated along the lines described by the full Eqs. (2)–(13) above.

3. Results

3.1. A program simulating the signal generation and processing

A computer program has been written in the numerical script language MATLAB to simulate the

Table 1
Parameters employed to simulate the wavelength modulated signals

Parameter	Value
Atomic mass, M_{atom}, (u)	85.5
Buffer gas mass, M_{buffer}, (u)	39.9
Temperature, T, (K)	2500
Pressure, P, (Pa)	1.01×10^5
Peak absorption cross-section, σ_0, (m^2)	100×10^{-20}
Interaction length, L, (m)	0.1
Wavelength, λ, (nm)	780
Collisional cross-section, σ_{coll}, (m^2) [a]	250×10^{-20}
Ramp frequency (Hz)	1
Ramp length (GHz)	25
Modulation frequency, f_m (Hz) [b]	10/1000

[a] The collisional cross-section is taken from p. 745 in Ref. [15] and represents the effective collisional cross-section for line broadening for the 780 nm transition of Rb atoms in an air/acetylene flame.

[b] The modulation frequency is 10 Hz for the curves presented in Figs 3, 4(a), (b), 5(a), (b), 6(a), (b), and 7, while it is 1 kHz for the others.

absorption profiles and the wavelength modulated signals under a variety of conditions. Since both collision and Doppler broadening can be present, the program calculates a Voigt absorption profiles (as a convolution of a Lorentzian and a Gaussian profile) for a given temperature and collision surrounding of the atoms. The laser is modulated by a sinusoidal signal, according to Eq. (2), producing a detector signal, following Eq. (8). The *2f*-harmonic signals are calculated according to Eqs. (11)–(13) utilizing a smoothing procedure consisting of a 5th order Butterworth filter. The values of the parameters that are common for all the simulations of the *2f*-signals are shown in Table 1. Typical values for temperature, pressure, absorption cross-section, and collisional broadening for atoms in a high temperature atomizer (e.g. a flame or a furnace) are used [15]. The simulation is general in the respect that it can represent any transition, although it has made use of some parameters (e.g. wavelength) of the 780 nm transition in Rb ($5s^2S_{1/2} - 5p^2P_{3/2}$). The program treats, however, only one single transition (with no hyperfine- or isotope splitting). The influence of hyperfine or isotope splitting is studied in more detail in a subsequent paper [11].

3.2. Unmodulated absorption profiles

Fig. 1 shows the typical line profiles for pure Lorentzian, Gaussian, and Voigt shapes as a function of frequency, as simulated by the computer program for conditions given in Table 1. The actual expressions used for estimates of the Lorentzian and Gaussian widths (and hence the Voigt profile) are

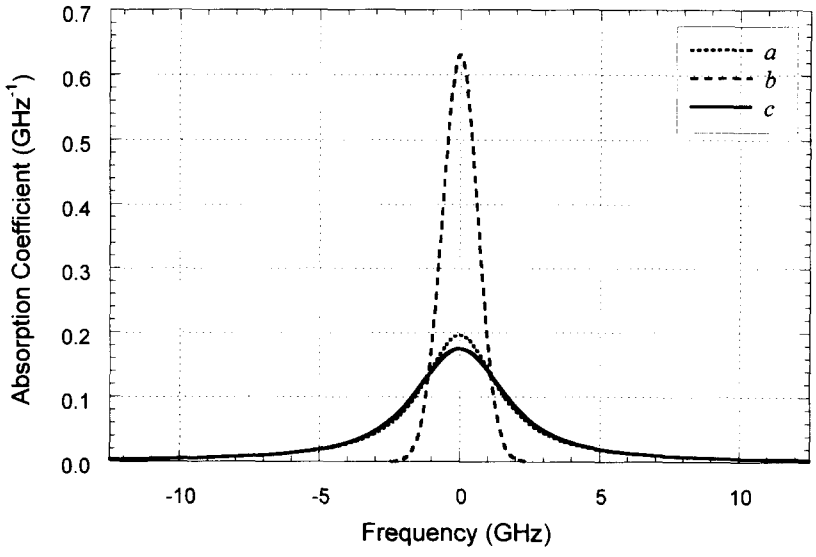

Fig. 1. Typical line shapes for pure Lorentzian, Gaussian, and Voigt distributions (curves a, b, and c, respectively) calculated from expressions given in Appendix A, using parameter values from Table 1. The widths (HWHM) of the three distributions are 0.75, 1.6, and 1.9 GHz, respectively, representing a typical case for atoms in a hot gas surrounding, e.g. a flame or a graphite furnace.

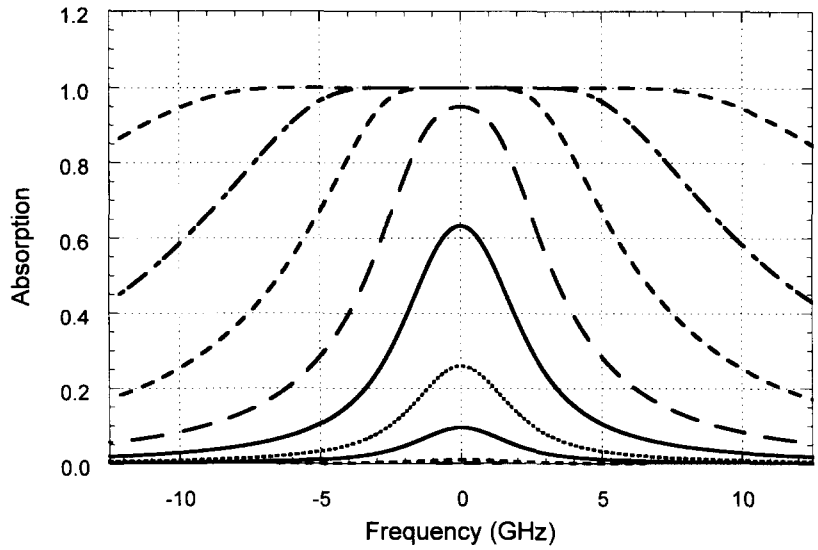

Fig. 2. Absorption profiles (according to Eqs (3) and (4), with $\chi(\nu)$ being a pure Voigt line-shape function, following Eqs. (A6)–(A8) in Appendix A) for atoms in a variety of optical densities. The nine curves refer to (from top to bottom) optical densities of 100, 30, 10, 3, 1, 0.3, 0.1, 0.01 and 0.001, respectively. The maximum absorption for an optical density of 1 is thus 0.63.

given in Appendix A. As can be seen from this figure, the collisional broadening width (the Lorentzian width) is smaller than the Gaussian width, describing a typical situation of atomization in a graphite furnace in a noble gas atmosphere. The general behaviour of the *2f*-wavelength modulation signals presented below is, however, not critically dependent upon the actual choice of broadening.

Fig. 2 presents the absorption profiles (according to Eqs. (3) and (4) with a pure Voigt profile as line-shape

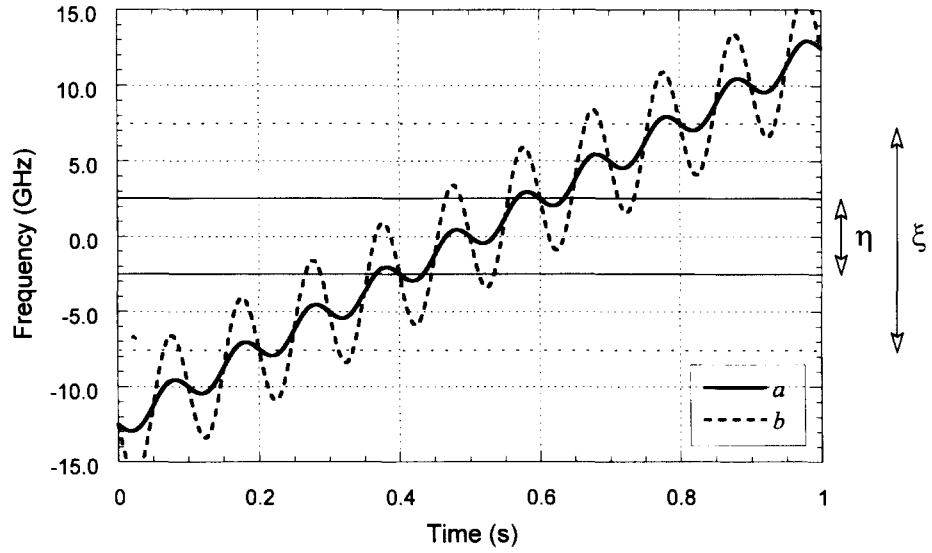

Fig. 3. Instantaneous wavelength (frequency) modulation schemes for the laser light. Curve a displays a situation with a frequency modulation amplitude of 1 GHz, while curve b shows the corresponding situation with a frequency modulation amplitude of 4 GHz. The modulation frequency is 10 Hz while the ramping rate of the center frequency is 25 GHz s^{-1}. The FWHM of two typical absorption profiles (for low optical densities and for an optical density of 10 from Fig. 2) are indicated by the greek letters η and ξ, respectively.

function) as a function of laser light frequency (expressed as the difference between the frequency of the laser light, ν_c, and the center absorption frequency of the atom, ν_0). The nine curves refer (from top to bottom) to optical densities ranging from 100 down to 0.001 (with the one with an optical density of 1 as the fifth curve, drawn by a solid line). It is well-known from ordinary atomic absorption measurements (e.g. using light produced by hollow cathode lamps) that detection of elements under conditions of optical densities above 1 results in poor precision and accuracy. Measurements in situations with optical densities above 3 is almost impossible to perform. We will below display the ability of the

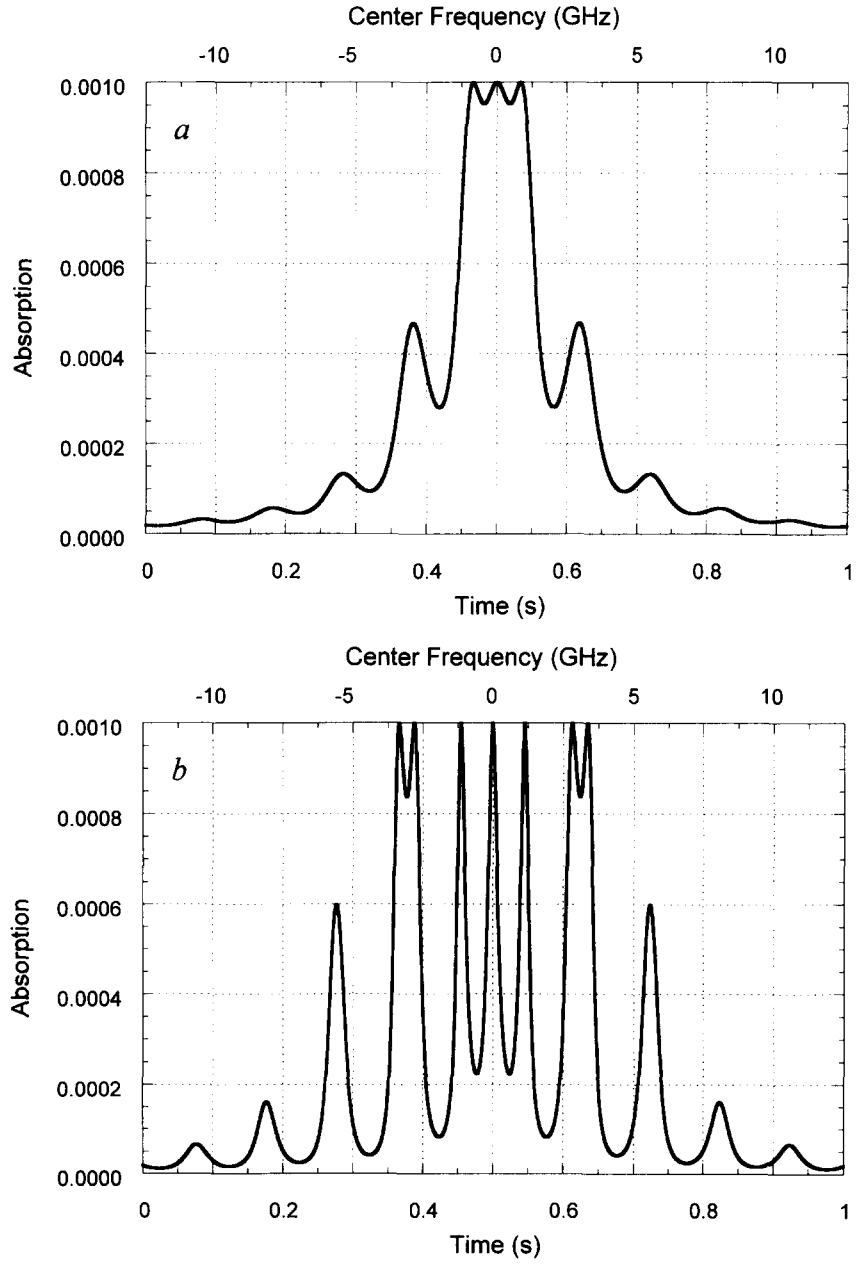

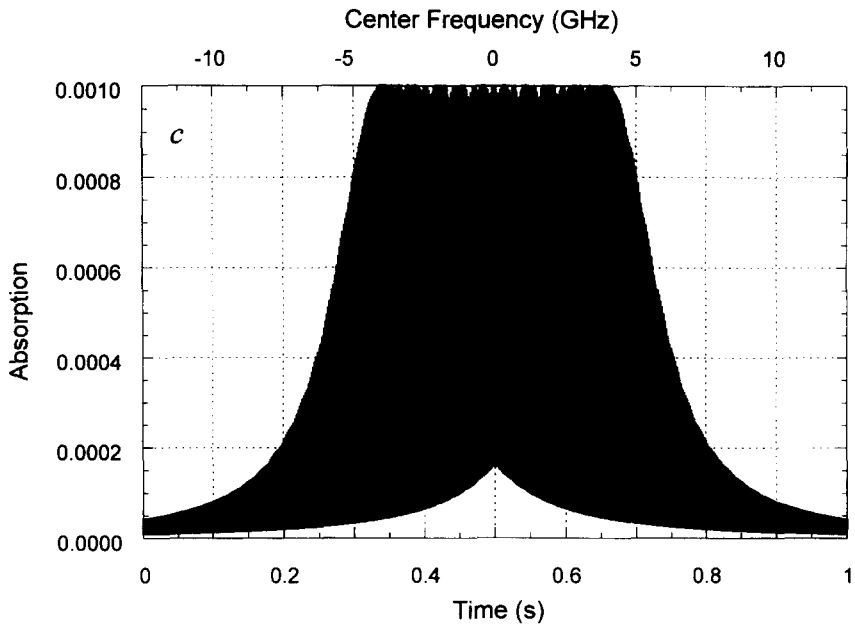

Fig. 4. Instantaneous absorption as a function of time (also expressed as the laser light center frequency, defined as the difference between the center frequency of the sinusoidally modulated laser light, ν_c, and the center absorption frequency of the atom, ν_0 at the top of the figure) under optically thin conditions (O.D. = 0.001). (a) and (b) correspond to the same modulation conditions as for curves a and b in Fig. 3, respectively, while (c) represents the case with ν_{mod} = 4 GHz and f_m = 1 kHz.

2f-WM technique to detect atoms also under conditions of high optical densities.

3.3. Time-dependent absorption signals

Fig. 3 shows a blow-up of two different wavelength (frequency) modulation schemes that can be obtained by a combination of Eqs. (2) and (15). For reasons of clarity, the modulation frequency is very low (10 Hz). Curve *a* corresponds to a case when the modulation amplitude is 1 GHz, while curve *b* represents a situation when it is 4 GHz. In all curves, the laser light center frequency is swept over a 25 GHz interval (i.e. the ramp length) during a period of 1 second. Hence, the ramp rate is 25 GHz/s.

The effects of these modulations of the laser wavelength (frequency) on systems with different optical densities are shown in Figs 4–6. The three figures correspond to systems with optical densities of 0.001, 10 and 100, respectively (i.e. the ninth, third and first curves in Fig. 2, respectively).

Each figure consists of three curves. The uppermost curves (i.e. Fig. 4(a), Fig. 5(a) and Fig. 6(a)) display the instantaneous absorption (according to Eq. (5)) following modulation of the laser light according to curve *a* in Fig. 3. One can clearly see that the absorption is affected by the wavelength modulation of the laser light, resulting in three almost similarly high peaks (close to the center frequency) for the case of low optical density (Fig. 4(a)), and a more flattened profile (around the center frequency) but modulated absorption on the flanks for the two other cases (Fig. 5(a) and Fig. 6(a)) corresponding to higher optical densities.

The shape of Fig. 4a can be understood by a comparison of the wavelength (frequency) modulation scheme displayed as curve *a* in Fig. 3 with the atomic absorption profile for an optically thin media (O.D. = 0.001). The FWHM of an atomic absorption profile under optical thin conditions has been indicated by the double arrow marked η in Fig. 3. One can (from curve *a* in Fig. 3) thus understand the origin of the three uppermost peaks in the spectrum displayed as Fig. 4a (curve *a* in Fig. 3 crosses the 0 level at three instances, at 0.46, 0.50, and 0.54 s, respectively). It is also clear that the two peaks at approximately half the maximum

height in Fig. 4(a) originates from the local maximum and minimum at 0.38 and 0.62 s in curve *a* in Fig. 3.

The situation shown as curve *a* in Fig. 3 (corresponding to the three uppermost curves in Figs 4–6) is, however, normally not typical for real experimental conditions but serves merely as an illustrative examples of the signal processing and behaviour in the *2f*-WM modulation technique. A somewhat more realistic situation is shown by curve *b* in Fig. 3, in which the modulation amplitude has been increased to 4 GHz (i.e. $\nu_{mod} = 4$ GHz). The three middle curves in the Figs 4–6 (i.e. (b) for each) correspond to the three systems of atoms (i.e. with optical densities of 0.001, 10 and 100, respectively) exposed to laser light

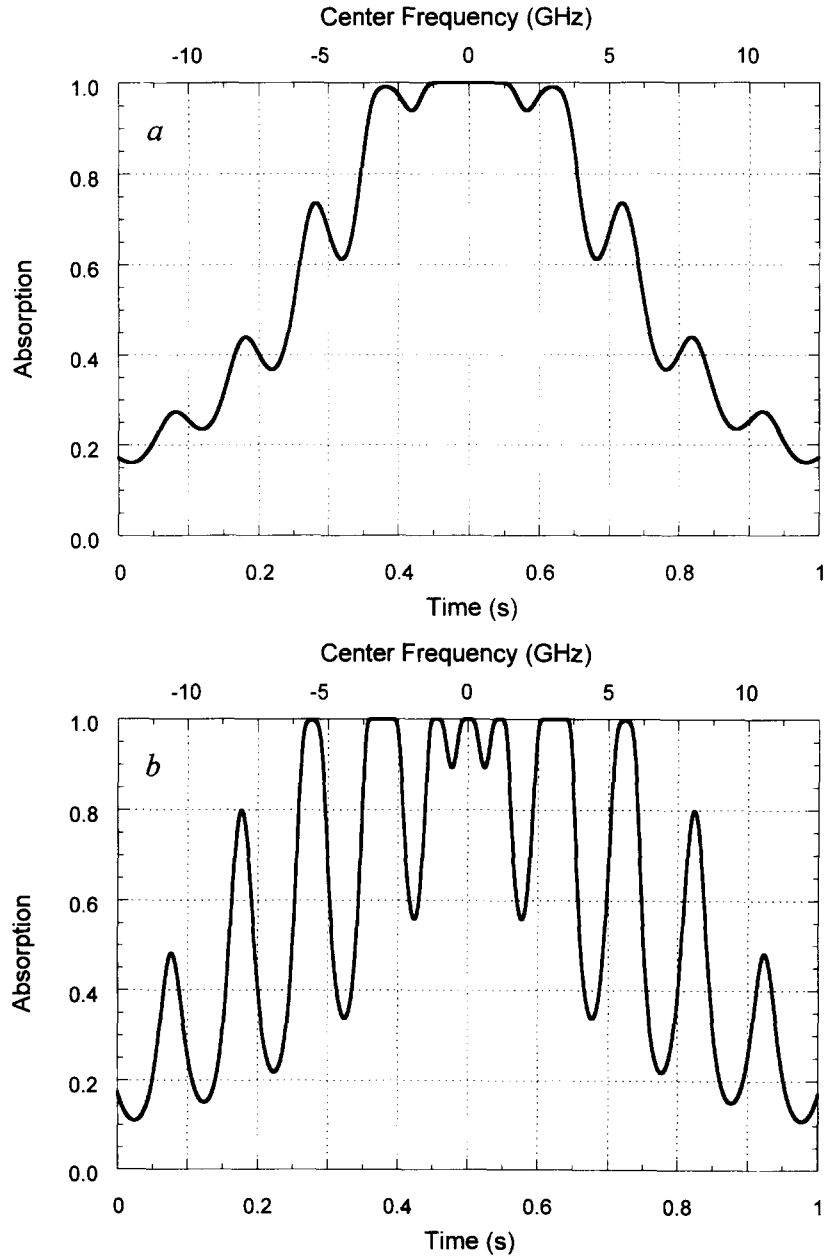

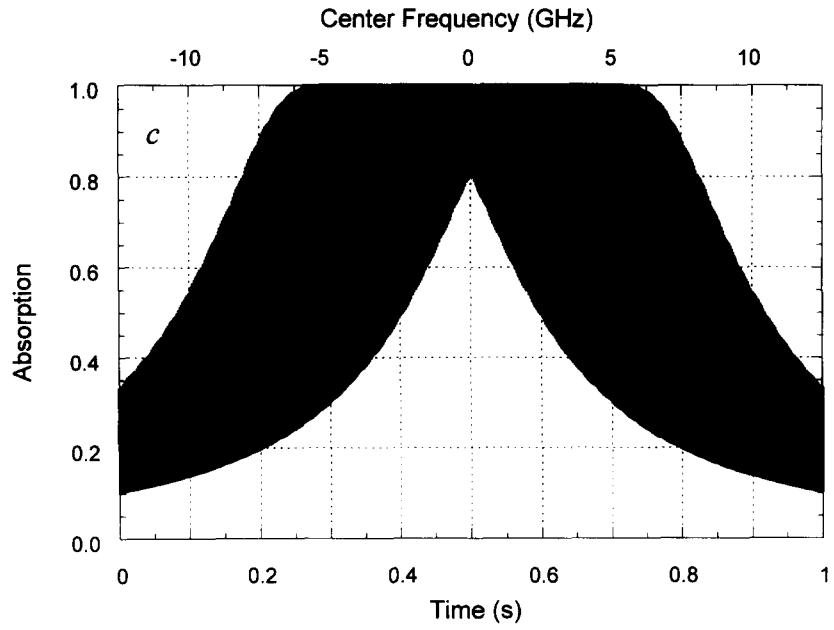

Fig. 5. Instantaneous absorption as a function of time under optically thick conditions (O.D. = 10). The three curves refer to the same modulation conditions as those in Fig. 4.

modulated according to curve *b* in Fig. 3. Since the HWHM of the Voigt profile is around 2.4 GHz in these simulations, this modulation amplitude is closer to that for which the signal takes its maximum value (which is $m \approx 2.1$–2.2 according to Silver [1]). One can in these three middle curves in Figs 4–6 still perceive the general absorption profile although the form of the curves are more complex. A close scrutiny of the curve in Fig. 4(b) shows that it consists of 7 peaks of virtually the same amplitude. Again referring to the wavelength (frequency) modulation scheme displayed as the curve *b* in Fig. 3, one can get an explanation for their origin (the laser frequency modulation curve crosses the 0 level 7 times). Also the other modulation periods of the curve *b* in Fig. 3 have parts that are within the FWHM of the absorption profile (which is marked by the letter ξ in Fig. 3). The other peaks (three on each side) in curve *4b* thus originate from the 'close encounters' in curve *b* in Fig. 3 (e.g. at 0.72, 0.82 and 0.92 s).

It is also interesting to note that while the signal is fairly flat around the center frequency for an optical density of 10 for a small modulation amplitude (Fig. 5(a)), a structure starts to be evident when the frequency modulation amplitude is larger (Fig. 5(b)). The modulation amplitude is, however, not sufficient to eliminate the flatness of the case with highest optical density (O.D. = 100), as can be seen in Fig. 6(b).

In addition, in order to benefit the most from the wavelength modulation technique, the modulation frequency should be significantly higher than 10 Hz. Such a situation is displayed in the three lowermost curves (Fig. 4(c), Fig. 5(c) and Fig. 6(c)) which all refer to a situation in which modulation frequency has been increased to 1 kHz, still with a modulation amplitude of 4 GHz (i.e. f_m = 1 kHz and ν_{mod} = 4 GHz). In this case, the time-dependent absorption signals are quite complex. From the case with low optical density, i.e. Fig. 4(c), it is difficult to apprehend that this feature is due to one single transition (which however is somewhat clearer from the case with the higher optical densities, Fig. 5(c) and Fig. 6(c)).

3.4. The read-out process

Fig. 7 shows the absorption profiles for both optically thin as well as thick conditions (i.e. optical

densities of 0.001, 10 and 100) for a frequency modulation situation displayed as curve *b* in Fig. 3 together with a *2f*-reference signal (the upper curve in each figure) for illustrative purposes. Fig. 8 shows the $\bar{S}_{2f-x}, \bar{S}_{2f-y}$, and $\bar{S}_{2f-r}$ signals (see Eqs. (11)–(13)) that result from a time integration of the product of the measured signal and the reference signal (corresponding to the output signals from the lock-in). The phase of the reference signals displayed in Fig. 7 has been chosen so that the integrated outputs correspond to the $\bar{S}_{2f-y}$ signals (according to Eq. (12)). As can be seen from Fig. 8, the $\bar{S}_{2f-y}$ signals are symmetrical around the peak of the absorption line and have (under low optical density conditions) their

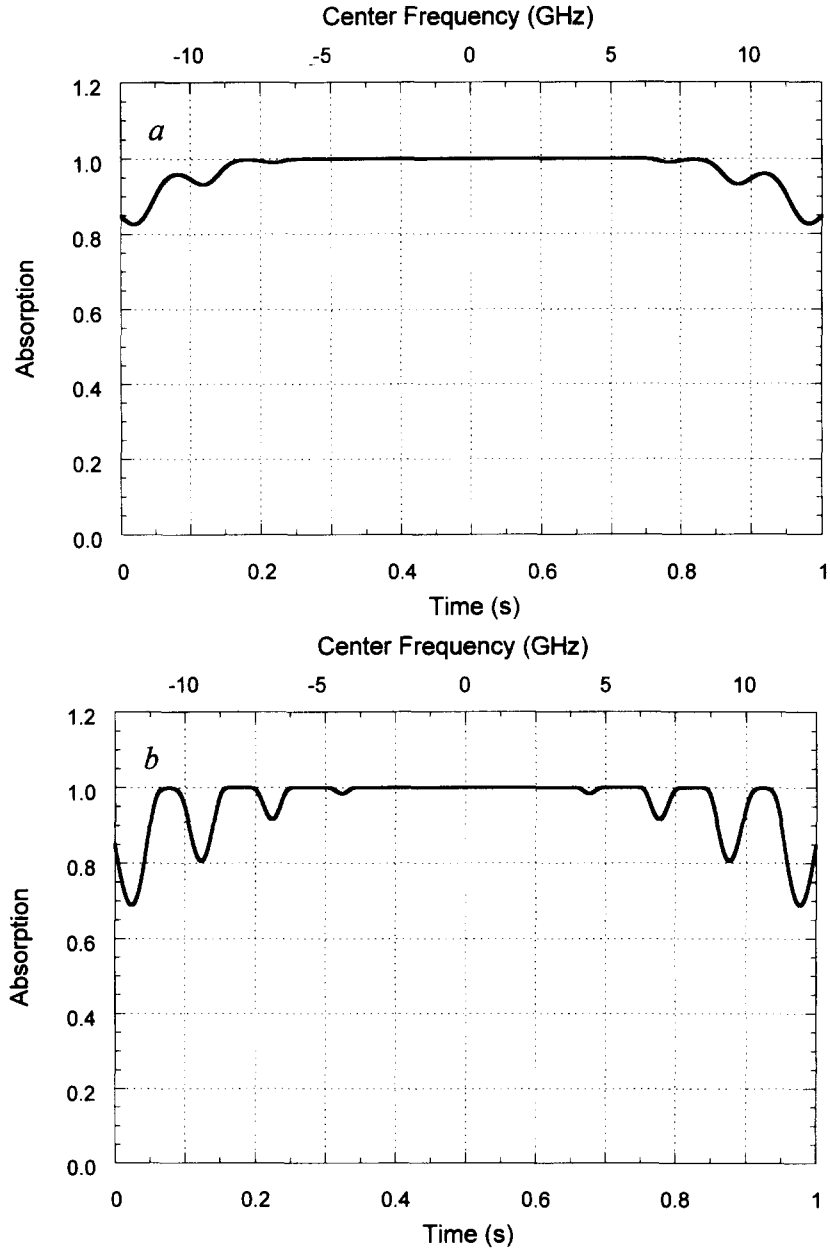

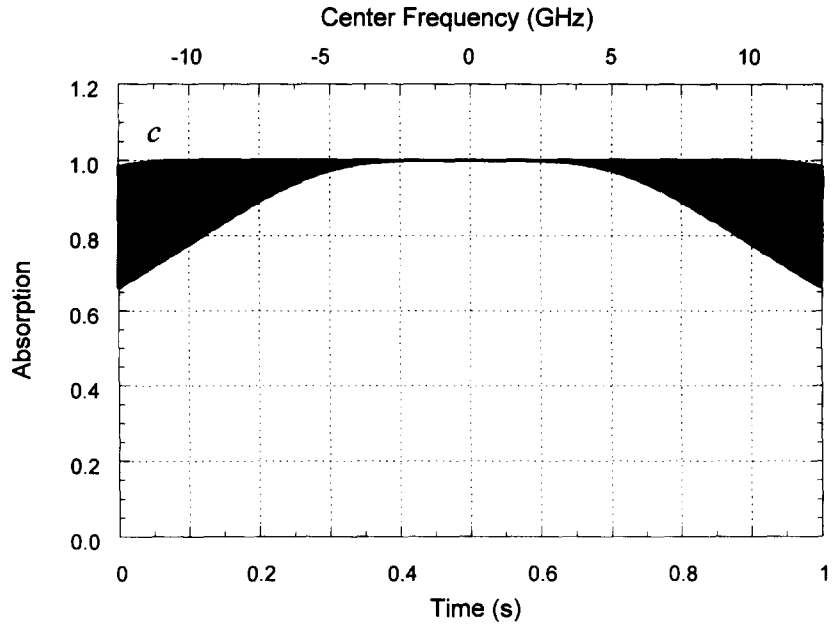

Fig. 6. Instantaneous absorption as a function of time under optically thick conditions (O.D. = 100). The three curves refer to the same modulation conditions as those in Fig. 4.

maximum values at the peak of the absorption profile while the $\bar{S}_{2f-x}$ is virtually equal to zero for all times, whereby the $\bar{S}_{2f-r}$ signal ends up being equal to the absolute value of $\bar{S}2_{f-y}$.

It is now possible, from the curves in Fig. 7, to obtain an qualitative understanding of why the $\bar{S}_{2f-y}$ signal from a single optical transition (e.g. that displayed in Fig. 1) is composed of a positive peak flanked by two negative peaks under optically thin conditions. As can be seen by a comparison of the signal curve with the *2f*-reference curve in Fig. 7(a), the signal curve and the reference signal are fully in-phase around the center frequency, giving rise to a positive $\bar{S}_{2f-y}$ signal, while they are fully out-of-phase a few GHz away (e.g. after 0.72 s), giving rise to a negative $\bar{S}_{2f-y}$ signal. The $\bar{S}_{2f-r}$ signal is often the practically preferred choice (in comparison with the $\bar{S}_{2f-y}$ signal) since it is independent of any uncontrolled phase shift between the detector and reference signals.

From an inspection of the two lowermost figures in Figs 7 and 8, it is clear why the *2f*-signals decrease to zero close to the resonance frequency under optically thick conditions (the optical density of the atom cloud is so high that no modulation of the signal is obtained at or around the center frequency). But, in the same way, it becomes clear that there is still a possibility to detect (and quantify) the density of atoms by studying the signal shapes at the wings of the absorption profiles (despite an optical density of 100). One can also see (from Fig. 8(b)) that the $\bar{S}_{2f-r}$ signal in fact consists of four peaks, all symmetrically placed with respect to the center wavelength. The same is, of course, valid for the case represented in Fig. 8(c), although the two outermost peaks are placed outside the shown interval. This concept is investigated in more detail in a coming paper [12].

3.5. 2f-wavelength modulated signals

3.5.1. The 2f-signals for various optical thicknesses

Fig. 9 compares the second harmonic wavelength modulated outputs (the $\bar{S}_{2f-r}$ signals) from absorption signals for a variety of optical densities (from 0.1 to 30). It is from this figure possible to study how the $\bar{S}_{2f-r}$ signal transforms from a three peaked spectrum (for the lowest optical densities) to a four peaked

spectrum (for higher optical densities). One can also notice that the side maxima are moving outwards, the higher the optical density. Despite from the fact that it makes the spectra more complex, this can be used to quantify and characterize high optical density media. Hence, it vouches for a possibility to expand the dynamic range of the wavelength modulated laser-diode absorption technique towards detection of higher atomic densities. An application of this process (applied to detection of ng amounts of atoms in graphite furnaces which give rise to very high concentrations of atoms under short time intervals) is considered in a separate paper [12].

3.5.2. The effects of the modulation amplitude upon the 2f-signals

As could be concluded from the examples shown in Figs 4–6, the frequency modulation amplitude (index) plays an important role in the signal generation process. It is therefore of interest also to investigate the influence of the frequency modulation index upon various signals.

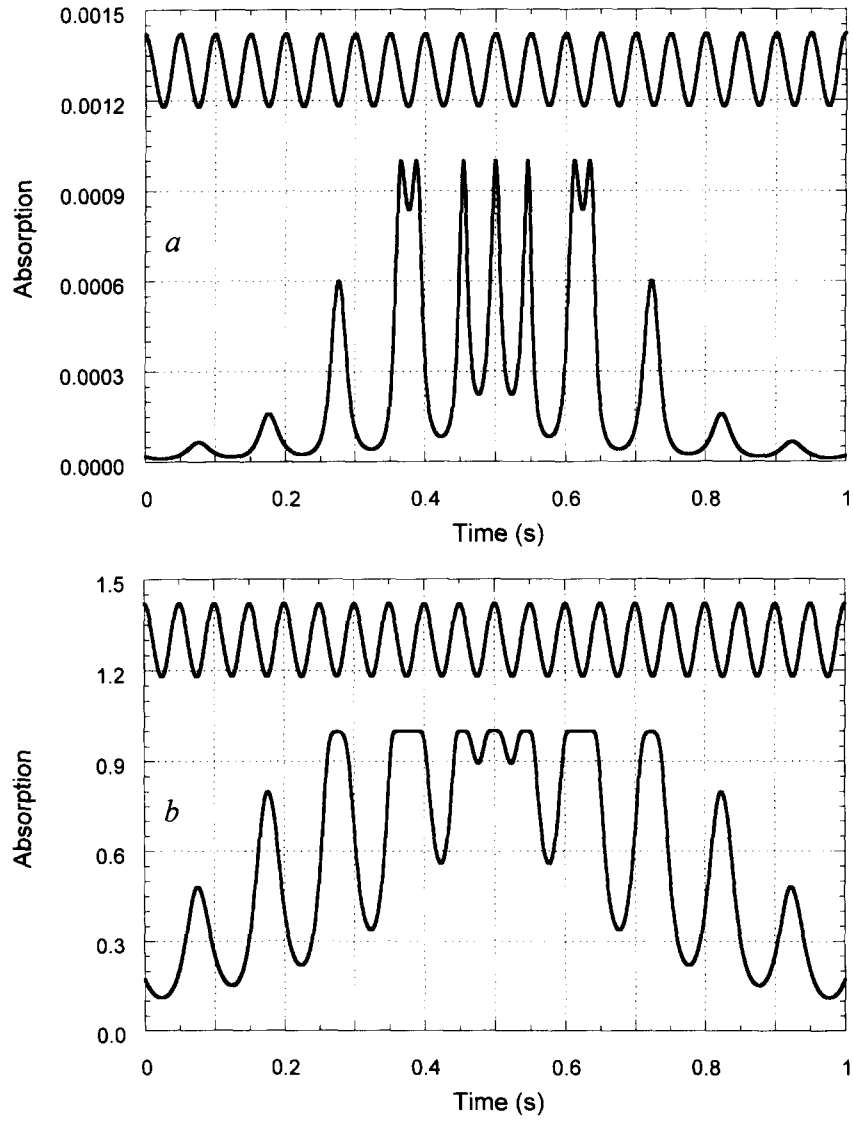

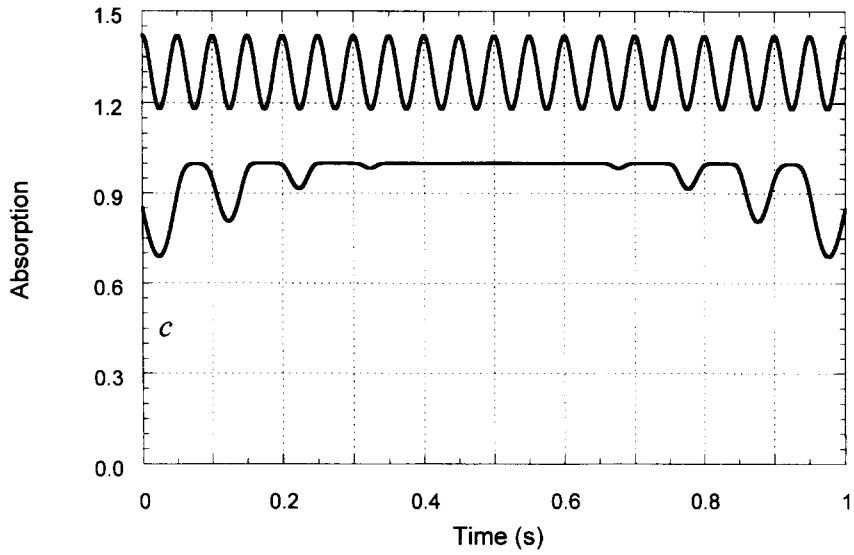

Fig. 7. Instantaneous absorption as a function of time for atoms under three different optical densities (0.001, 10 and 100 for (a), (b) and (c), respectively). The modulation conditions are those of curve b in Fig. 3. The upper curves in each figure are the *2f*-reference signals (whose phase has been chosen as $\pi/2$, implying that the integrated output signals will correspond to the $\bar{S}_{2f-y}$ signals).

Fig. 10 shows a number of *2f*-signals ($\bar{S}_{2f-r}$) for optical densities equal to 0.001, and 10 in Figs. 10(a) and (b), respectively, for a variety of modulation amplitudes.

From Fig. 10(a), which shows the case for optically thin conditions (O.D. = 0.001), one can see that the *2f*-WM signal ($\bar{S}_{2f-r}$) first increases and then decreases (at the center frequency) as the frequency modulation amplitude is being increased (as previously has been pointed out in the literature by Silver [1]), with a maximum of the $\bar{S}_{2f-r}$ signal for curve *c* which has a frequency modulation amplitude (4 GHz) corresponding to a modulation index of $m \approx 2.1$ (which is in accordance with predictions [1]). It can also be observed that the signal becomes broader and more distorted as the frequency modulation amplitude becomes larger. In addition, for large frequency modulation amplitudes (e.g. above 10 GHz), one finds that the maximum of the signal no longer is at the center frequency, but rather at the two satellite peaks, as can be seen from curve *d*.

Similarly, Fig. 10(b) shows that for an optical density equal to 10, the maximum value of the $\bar{S}_{2f-r}$ signal at the center wavelength is obtained for modulation amplitudes around 14 GHz. The latter amplitude also corresponds to a modulation index of about 2.1 (since the absorption profile for a distribution of atoms with an optical density equal to 10 has a HWHM of about 6.6 GHz). This time, however, it should be observed that the profile consists of four peaks (and thus a minimum at the center frequency) for the lowest modulation amplitudes while it has a three-peak structure at higher modulation amplitudes.

3.5.3. Curve-of-growth for 2f-wavelength modulated signals

Fig. 11 presents the *2f*-WM signal strengths ($\bar{S}_{2f-r}$) as a function of optical density for a variety of detunings for three different frequency modulation amplitudes (ν_{mod} = 4, 10 and 14 GHz, displayed as (a), (b) and (c), respectively). The six curves in each figure correspond to detunings of the center frequency of the laser from that of the atomic species of 0, 2.5, 5.0, 7.5, 10 and 12.5 GHz.

The frequency modulation amplitude used in Fig. 11(a) gives the maximum signal at low optical densities (i.e. ν_{mod} = 4 GHz and m = 2.1), while those in Fig. 11(b) and (c) (ν_{mod} = 10 and 14 GHz, respectively) give maximum signals for higher optical densities (e.g. 14 GHz gives a maximum signals for O.D. = 10).

It can be observed from the figures that all the signals first increase with optical density, up to a maximum value (whose position depends on the choice of detuning), after which they again decrease. Some of the curves (the ones for highest detunings for each frequency modulation amplitude) will experience yet another increase-and-decrease-cycle as a function of optical density. Hence, the curve-of-growth is far from a single-valued function as a function of optical density. This might at first be seen as an inconvenience but can be used to determine optical thicknesses with high accuracy also for optical densities far above unit (as is discussed in more detail in the accompanying paper [12]). One can also notice that

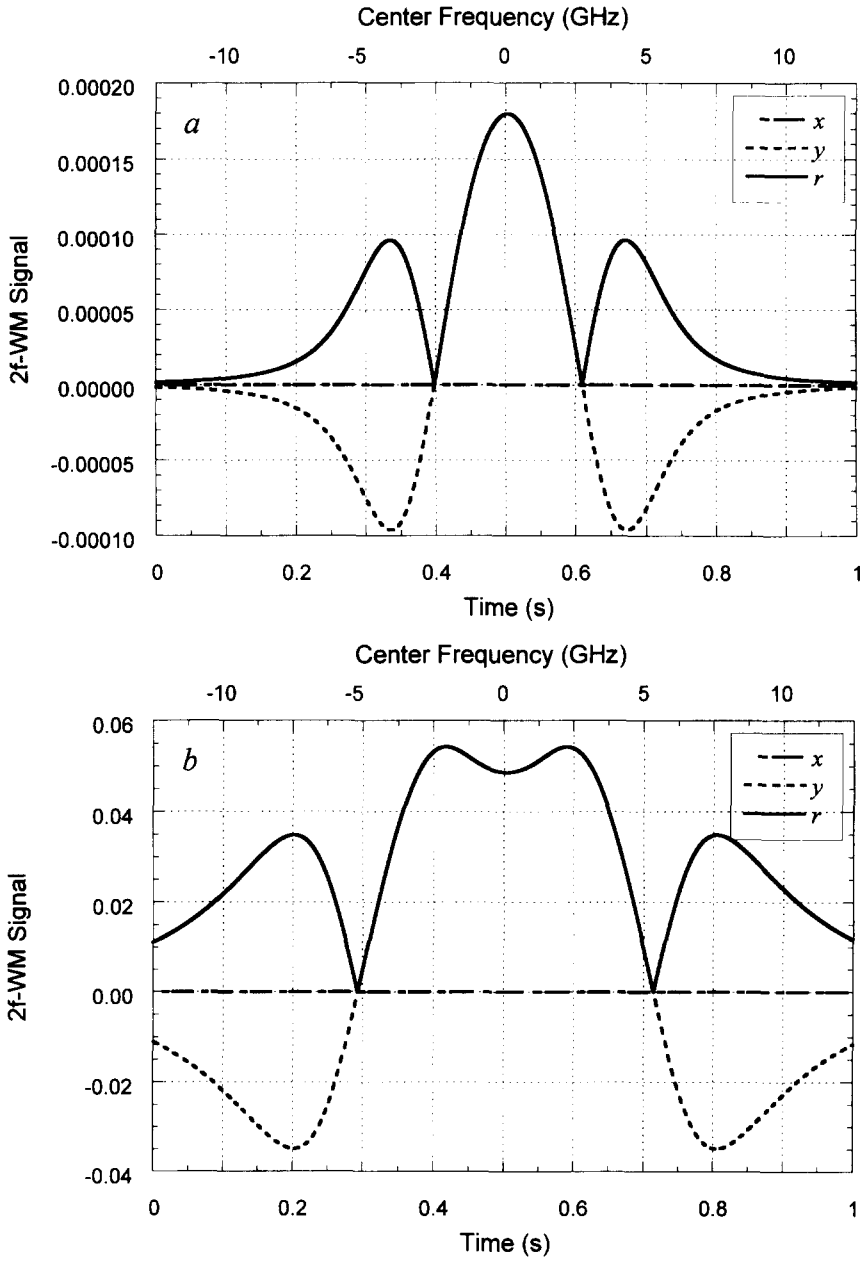

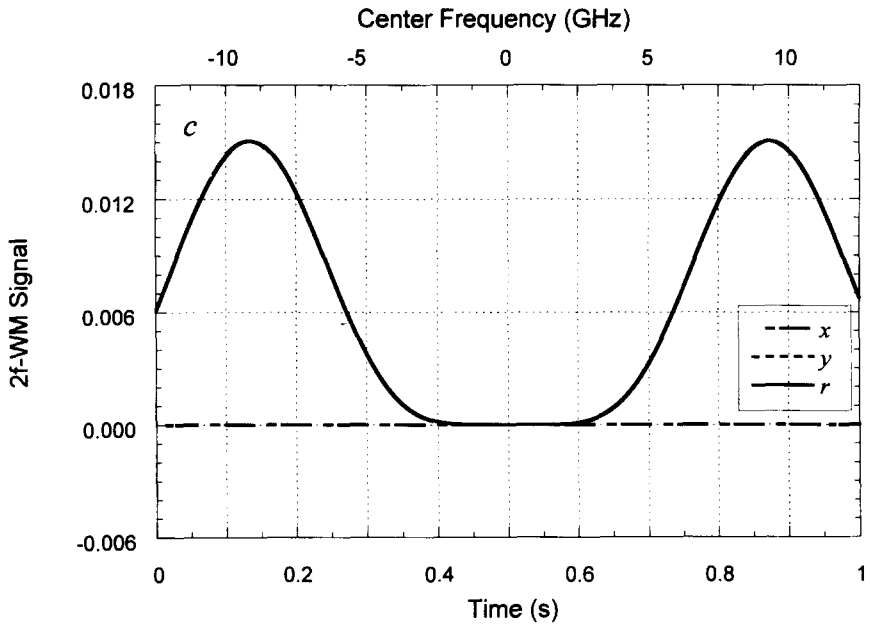

Fig. 8. Second harmonic wavelength modulated outputs, i.e. 2*f*-WM signals ($\bar{S}_{2f-x}$, $\bar{S}_{2f-y}$, and $\bar{S}_{2f-r}$) (i.e. those that correspond to the 2*f*-output from a lock-in amplifier) that result from the modulation process involving the measured modulated absorption and the 2*f*-reference signals for cases similar to those displayed in Fig. 7 (with the only difference being that they have been modulated by a 1 kHz frequency, as those in Fig. 4(c), Fig. 5(c) and Fig. 6(c)). For all curves, the $\bar{S}_{2f-x}$ signal is always equal to zero, whereas the $\bar{S}_{2f-r}$ signals are equal to the absolute value of the $\bar{S}_{2f-y}$ signal.

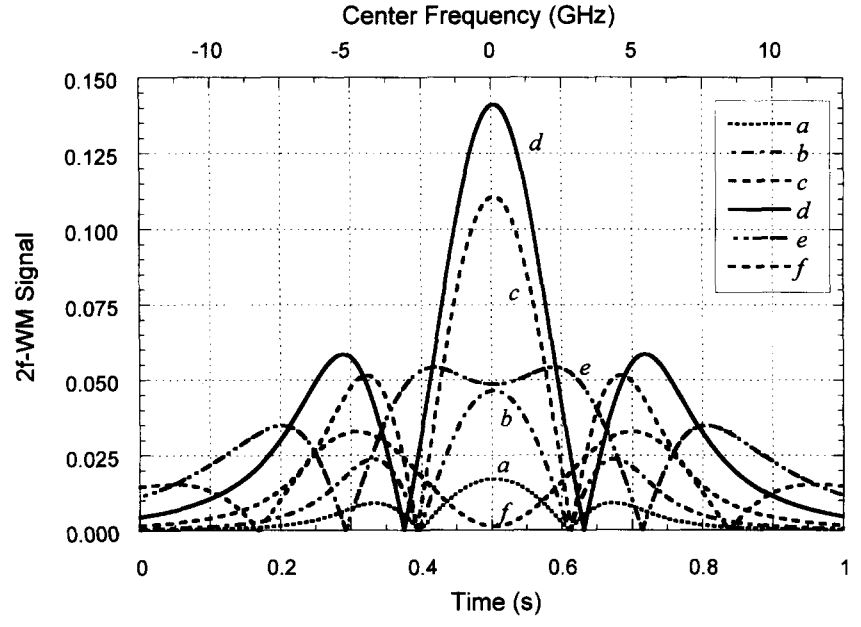

Fig. 9. 2*f*-WM ($\bar{S}_{2f-r}$) signals for a variety of optical densities. The eight profiles correspond to the following optical densities: curve a, O.D. = 0.1; curve b, O.D. = 0.3; curve c, O.D. = 1; curve d, O.D. = 3; curve e, O.D. = 10; and curve f, O.D. = 30. The frequency modulation amplitude is 4 GHz in all curves.

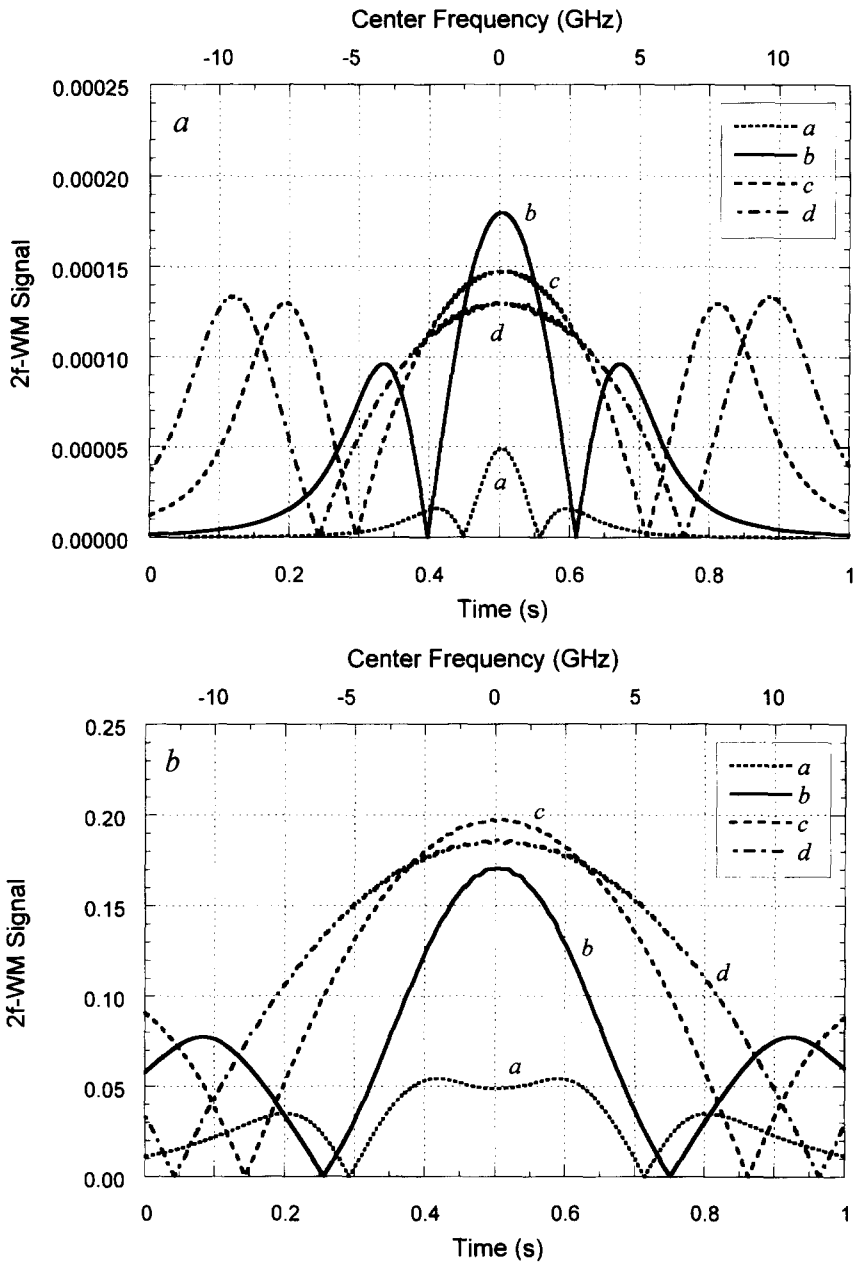

Fig. 10. 2*f*-WM ($\bar{S}_{2f-r}$) signals for a variety of modulation amplitudes for optical densities equal to 0.001 (a) and 10 (b). The various curves in the two figures correspond to the following modulation amplitudes (with modulation index within parentheses): (a) curve a, ν_{mod} = 1 GHz (m = 0.5); curve b, ν_{mod} = 4 GHz (m = 2.1); curve c, ν_{mod} = 8 GHz (m = 4.2); curve d, ν_{mod} = 10 GHz (m = 5.2); (b) curve a, ν_{mod} = 4 GHz (m = 0.6); curve b, ν_{mod} = 8 GHz (m = 1.2); curve c, ν_{mod} = 14 GHz (m = 2.1); curve d, ν_{mod} = 18 GHz (m = 2.7).

the curve-of-growth increases and decreases most rapidly for the resonant case (i.e. for the curves *a* in each figure).

The origin of the dual-valued functionality of the lowest detuning curves can be understood by an inspection of Fig. 9. At the center frequency, one can clearly see that the signal first increases with optical density (up to a maximum which for Fig. 9 is represented by curve *d*, i.e. an O.D. of 3) after which it decreases again. The reason for the decrease is, of course, that the absorption profile is broadened to such an extent that its curvature (at the atomic transition frequency) starts to decrease. The same argument holds for curve *b* in Fig. 11(a), i.e. for a frequency modulation amplitude of 4 GHz and a detuning of 2.5 GHz.

The fact that the other curves *c*–*f* in Fig. 11(a) show yet another increase-and-decrease-cycle as a function of optical density can also be understood from a comparison with Fig. 9. Taking curve *c* in Fig. 11(a) as an example (with a detuning of 5 GHz) one can from Fig. 9 see that the first increase-and-decrease-cycle has the same origin as those of the curves *a* and *b*. As the optical density increases, however, the width of the absorption profiles increases (as is illustrated in Fig. 2) whereby the zero point of the $\bar{S}_{2f-r}$ signal (which is the point at which the $\bar{S}_{2f-y}$ signal crosses the *x*-axis, i.e. changes sign) will move 'outwards' (i.e. towards larger optical densities). As the optical density increases, this $\bar{S}_{2f-r}$ zero point position will eventually take the value of the detuning, after which it will continue 'outwards'. This thus explains the extra minimum in the $\bar{S}_{2f-r}$ signal-*vs*-optical density curves for the cases with highest detunings in Fig. 11. One can also conclude that dual increase-and-decrease-cycles will appear whenever the detuning is larger than the HWBL (Half Width at the Base Line) of the $\bar{S}_{2f-r}$ signal at low optical densities.

This also explains the finding that the onset of dual increase-and-decrease-cycles takes place for higher detunings for larger frequency modulation amplitudes (Fig. 10 clearly shows that the HWBL of the $\bar{S}_{2f-r}$ signal increases with increasing modulation amplitude). Fig. 11(b) shows that the 5 GHz detuning produces only a single increase-and-decrease-cycle for a frequency modulation amplitude of 10 GHz, while Fig. 11(c), shows that the same is valid for a 7.5 GHz detuning for a frequency modulation amplitude of 14 GHz.

Fig. 12 shows the *2f*-WM signal strengths ($\bar{S}_{2f-r}$) as a function of optical density for a variety of frequency modulation amplitudes (i.e. ν_{mod}) for four different detunings ($\nu_c = \nu_0$, $\nu_c = \nu_0 + 2.5$, $\nu_c = \nu_0 + 5$, and $\nu_c = \nu_0 + 12.5$ GHz, displayed as (a)–(d), respectively).

Fig. 12 shows a similar behaviour to that in Fig. 11. The signals first increase with optical density to a maximum value (whose position depends upon the modulation index as well as the center frequency) after which they start to decrease again. As for Fig. 11, the curves with largest detuning (i.e. preferably those in Fig. 12(d)) show an additional increase-and-decrease-cycle (i.e. they have an extra minimum).

A close analysis of the low optical density region indicates that the *2f*-WM signal strength increases linearly with mass up to an optical density of 0.10. The reason for this is that the width of the effective absorption profile increases only by 3.5% for optical densities between 0.001 and 0.1. This implies that there will be a negligible variation on the effective modulation index for a given frequency modulation amplitude. This is the limiting case where the exponential in the expression for absorption Eq. (3), i.e. $\exp(-x)$, can be approximated by $1 - x$, wherefore the signal, both the pure absorption signal and the *2f*-WM ($\bar{S}_{2f-r}$) signal, will have a linear dependence with mass, which makes the second harmonic technique so useful for detection of ultra-trace amounts of analyte.

For the curves with no extra minimum the position of the maximum moves to higher optical densities the larger the frequency modulation amplitude. Again, a comparison with Fig. 9 explains why.

The extra minimum for some of the curves have the same origin as the minima in Fig. 11, i.e. the fact that the curves *a* and *b* in Fig. 12(c) have an extra minimum is that they refer to situations in which the frequency modulation amplitudes are so low that the HWBL in Fig. 10(a) is smaller than the detuning (in this case 5 GHz). The minima in Fig. 10 will move 'outwards' with increasing optical density (as can be seen from a comparison of Fig. 10(a) and (b)) thus resulting in the minima in Fig. 12(c). This also explains why all curves displayed in Fig. 12(d) (for which the detuning is significantly larger, 12.5 GHz) have an extra minimum (all curves in Fig. 10(a) have their minimum within 12.5 GHz).

4. Conclusion

We have in this paper investigated the use of the *2f*-Wavelength Modulation (WM) technique for detection of atoms under optically thin as well as optically thick conditions so as to assess the possibilities to utilize the technique also for detection of higher concentrations of species, i.e. for enlarging the dynamic range of the technique. Since no closed solutions exist for the signals strength of the *2f*-WM signal for non-thin optical conditions, the entire process of laser light modulation, the atomic absorption and signal convolution has been simulated by the use of a computer program.

We have described, in detail, the origin of the ordinary three-peak structure of the *2f*-WM ($\bar{S}_{2f-r}$) signal (for a tuning of the center frequency of the laser light, around which it is rapidly modulated). The simulations clearly show that this three-peak structure transposes into a four-peak structure (with a local minimum at the center frequency) when higher masses are detected (i.e. for higher optical densities).

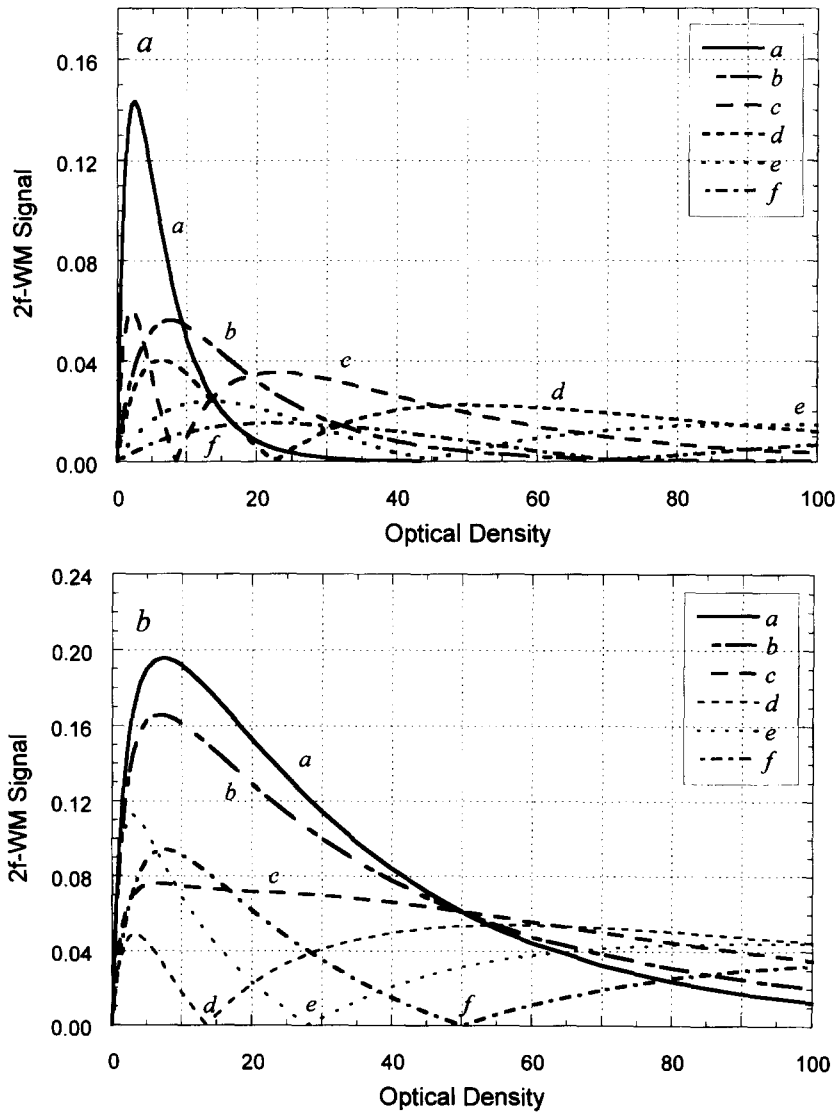

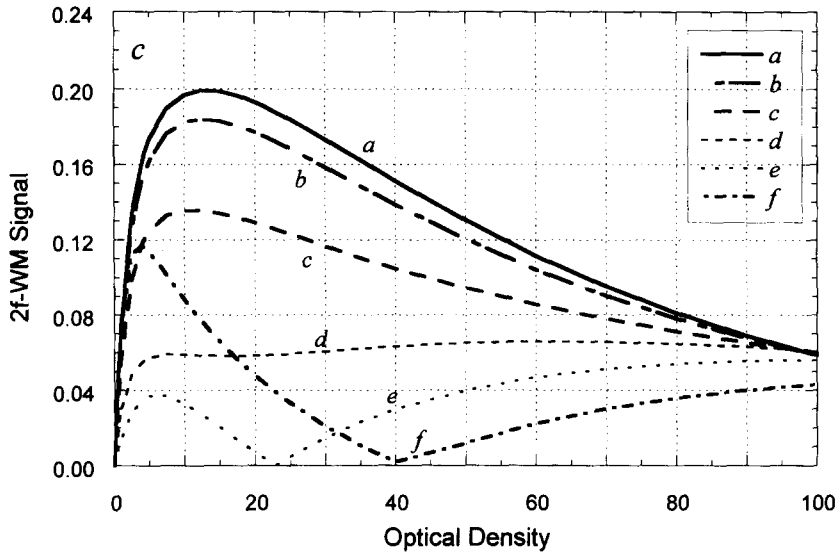

Fig. 11. 2*f*-WM signal strengths ($\bar{S}_{2f-r}$) as a function of optical density for a variety of detunings for three different frequency modulation amplitudes (ν_{mod} = 4, 10 and 14 GHz for (a), (b) and (c), respectively). The six curves in each figure correspond to detunings of the laser center frequency from that of the atomic species of 0, 2.5, 5.0, 7.5, 10 and 12.5 GHz (marked with a, b, c, d, e, and f, respectively).

If the modulation index is optimized for the limit of low optical densities, as for trace element analysis, the 2*f*-WM ($\bar{S}_{2f-r}$) signal at resonance is a linear function of mass for low optical densities. For higher masses, however, a deviation from linearity results as a consequence of the broadening of the absorption profile. This effect will eventually result in a decrease of the signals with increasing mass (for sufficiently high optical densities, the 2*f*-WM ($\bar{S}_{2f-r}$) signal strength at the center frequency will even decrease to zero). It is explicitly shown that the 2*f*-WM ($\bar{S}_{2f-r}$) signal strength is not a single valued function as a function of optical density (since it has a maximum value).

A dual-valued function always appears whenever the detuning is sufficiently small, i.e. smaller than HWBL (Half Width at the Base Line) of the 2*f*-WM ($\bar{S}_{2f-r}$) signal under optical thin conditions. For larger detunings, the 2*f*-WM ($\bar{S}_{2f-r}$) signal strength is still a dual-valued function for high enough frequency modulation amplitudes. For larger detunings in combination with low frequency modulation amplitudes, the 2*f*-WM ($\bar{S}_{2f-r}$) signal strength is a quadrupled-valued function of optical density.

This behavior, which first might look awkward, can however, be used to enlarge the dynamic range of the 2*f*-WM ($\bar{S}_{2f-r}$) technique. The details of this, however, is studied in a separate paper [12].

Despite this, we have shown that it is possible to utilize the 2*f*-WM technique for detection of atoms under condition of high optical densities either by detuning the laser center frequency (around which the frequency is rapidly modulated) or by using increased frequency modulation amplitudes. If an increased frequency modulation amplitude is used, however, (thus optimized for a high optical density) a lower sensitivity will be obtained in the low optical density region.

In conclusions, we have shown, which is of highest importance, that the 2*f*-WM ($\bar{S}_{2f-2}$) technique allows the detection of atoms also under optically thick conditions that cannot be handled by direct measurements of the absorption at the central wavelength.

Acknowledgements

The authors would like to acknowledge the Swedish Institute (Sweden) and the Universidad de Los Andes, Merida, Venezuela for financial support for the visit of D.R. to the Laser Spectroscopy Group at Umeå University, Sweden. In addition, the authors

would also like to thank the Swedish Research Council for Engineering Sciences under project no. 251/94-544 for financial support.

Appendix A: Calculations of the Voigt profiles

The Doppler width (HWHM), $\Delta\nu_D$, is given by the expression

$$\Delta\nu_D = \nu \cdot 3.58\ 10^{-7} \frac{T}{M_{atom}} \quad \text{(A1)}$$

where ν is the frequency of the light (in Hz, i.e. c/λ), T is the temperature (in K) and the M_{atom} is the mass (in units of u) of the atom (Eq. 3.11.14 in Ref. [16]). The specific values of the various entities are given in the Table.

The collisionally induced width (HWHM), $\Delta\nu_L$, is given by (Eq. 3.9.11 in Ref. [16])

$$\Delta\nu_L = \frac{k_{coll}}{2\pi} \quad \text{(A2)}$$

where k_{coll} is the total collision rate (in Hz), given by

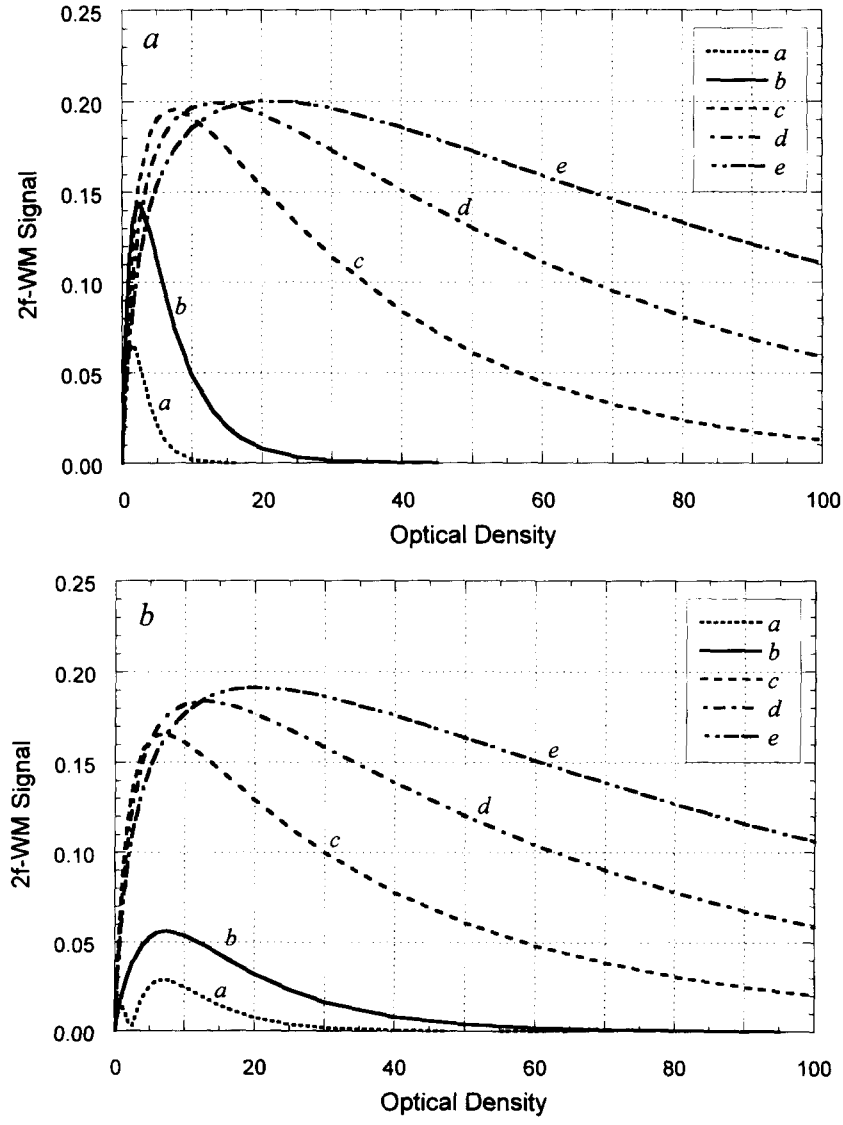

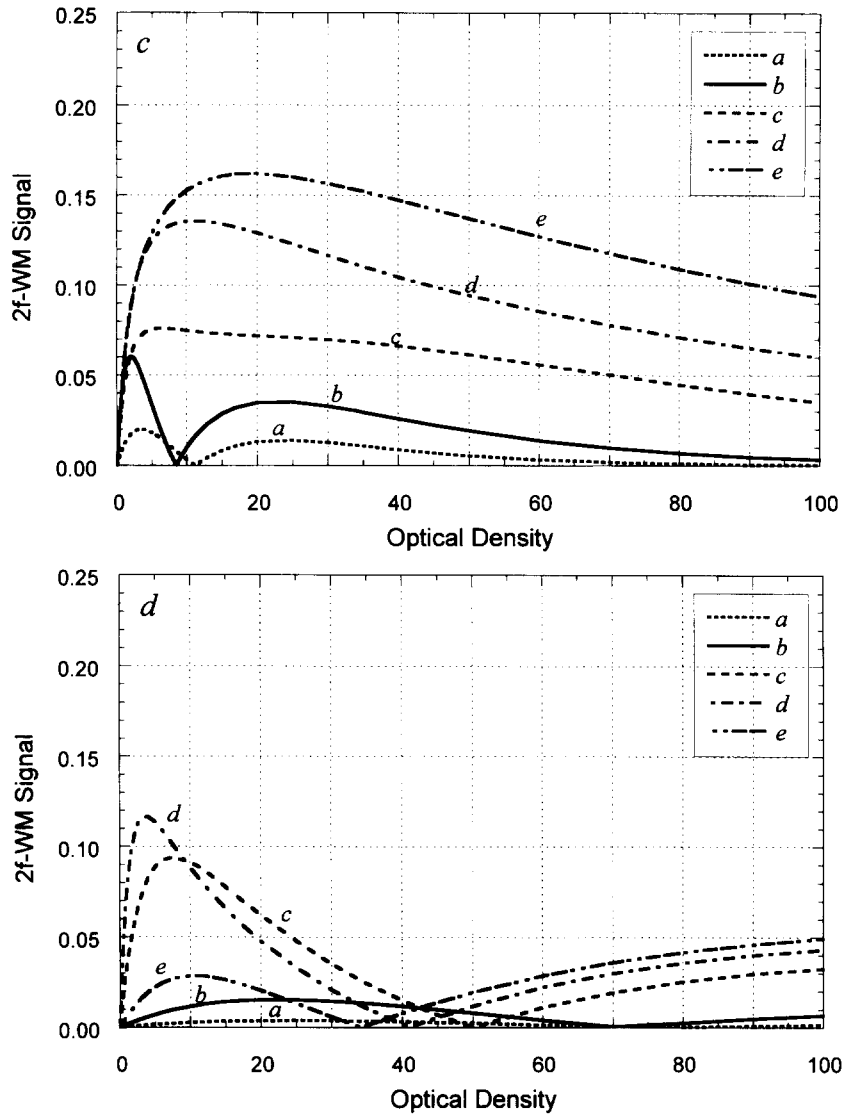

Fig. 12. 2*f*-WM signal strengths ($\bar{S}_{2f-r}$) as a function of optical density for five different frequency modulation amplitudes (ν_{mod} = 2, 4, 10, 14 and 18 GHz for the curves a, b, c, d, and e, respectively) for four different detunings, 0, 2.5, 5, and 12.5 GHz (for (a), (b), (c), and (d), respectively).

(Eq. 3.10.5 in Ref. [16])

$$k_{coll} = \rho_{buffer}\sigma_{coll}\nu_{rel} \tag{A3}$$

where, in turn, ρ_{buffer} is the density of buffer gas species (m^{-3}), given by

$$\rho_{buffer} = \frac{P}{kT}, \tag{A4}$$

σ_{coll} the collisional cross-section (m^2), and ν_{rel} the relative velocity between the atoms and the buffer gas species,

$$\nu_{rel} = \sqrt{\frac{8RT}{\pi}\left(\frac{1}{M_{atom}} + \frac{1}{M_{buffer}}\right)} \tag{A5}$$

The value of the collisional cross-section has been taken as 250 10^{-20} m^2, which corresponds fairly well to published values for Rb in flames (p. 745 in Ref [15]).

In the equations above, P is the pressure of the buffer gas species, k Boltzmann's constant (1.38×10^{-23} J/K), and R the molar gas constant (8314 J/(K kmol)).

The combined Voigt function can then be expressed (Eqs. 3.12.3–3.12.5 in Ref. [16]) as an integral as

$$V(\nu)=\frac{1}{\pi^{3/2}}\frac{b^2}{\Delta\nu_L}\int_{-\infty}^{\infty}\frac{e^{-y2}}{(a(\nu)+y)^2+b^2}dy \tag{A6}$$

where $a(\nu)$ and b are given by

$$a(\nu)=\sqrt{ln2}\frac{\nu_0-\nu}{\Delta\nu_D} \tag{A7}$$

and

$$b=\sqrt{ln2}\frac{\Delta\nu_L}{\Delta\nu_D}. \tag{A8}$$

References

[1] J.A. Silver, Frequency-modulation spectroscopy for trace species detection: theory and comparison among experimental methods, Appl. Opt. 31 (1992) 707–717.

[2] D.S. Bomse, A.C. Stanton, J.A. Silver, Frequency modulation and wavelength modulation spectroscopies: comparison of experimental methods using a lead-salt diode laser, Appl. Opt. 31 (1992) 718–731.

[3] J. Reid, D. Labrie, Second-harmonic detection with tuneable diode lasers — comparison of experiment and theory, Appl. Phys. B 26 (1981) 203–210.

[4] D.T. Cassidy, J. Reid, Atmospheric pressure monitoring of trace gases using tunable diode lasers, Appl. Opt. 21 (1982) 1186–1190.

[5] F. Slemr, G.W. Harris, D.R. Hastie, G.I. Mackay, H.I. Schiff, Measurement of gas phase hydrogen peroxide in air by tunable diode laser absorption spectrometry, J. Geophys. Res. 91 (1986) 5371–5378.

[6] D.M. Bruce, D.T. Cassidy, Detection of oxygen using short-extended-cavity GaAs semiconductor diode laser, Appl. Opt. 29 (1990) 1327–1332.

[7] P. Werle, F. Slemr, M. Gehrtz, C. Bräuchle, Quantum-limited FM-spectroscopy with a lead-salt diode laser, Appl. Phys. B 49 (1898) 99–108.

[8] K. Niemax, H. Groll, C. Schnürer-Patschan, Element analysis by diode laser spectroscopy, Spectrochim. Acta Rev. 15 (1993) 349–377.

[9] P. Ljung and O. Axner, Measurements of rubidium in standard reference samples by wavelength-modulation diode laser absorption spectrometry in a graphite furnace, Spectrochim. Acta Part B 52 (1997) 305-319.

[10] A. Zybin, C. Schnürer-Patschan, K. Niemax, Wavelength modulation diode laser atomic spectrometry in modulated low-pressure helium plasmas for element-selective detection in gas chromatography, J. Anal. At. Spectrom. 10 (1995) 563–567.

[11] J. Gustafsson, D. Rojas, and O. Axner, The influence of hyperfine structure and isotope shifts on the detection of Rb atoms in atmospheric pressure atomizers by the 2f-wavelength modulation technique. Spectrochimica Acta Part B (1997) In press.

[12] J. Gustafsson, N. Chekalin, D. Rojas, and O. Axner, Wavelength modulated laser diode absorption spectrometry for detection of atoms under optically thick conditions. Submitted to Spectrochimica Acta Part B, (1997).

[13] R. Arndt, Analytical line shapes for Lorentzian signals broadened by modulation, J. Appl. Phys. 36 (1965) 2522–2524.

[14] G.V.H. Wilson, Modulation broadenig of NMR and ESR line shapes, J. Appl. Phys. 34 (1963) 3276–3285.

[15] C.T.J. Alkemade, T. Hollander, W. Snelleman, and P.J.T. Zeegers, Metal Vapours in Flames. Oxford: Pergamon Press, 1982.

[16] P.W. Milonni and J.H. Eberly, Lasers. New York, New York: John Wiley and Sons, 1988.